JOINT INSTITUTE FOR NUCLEAR RESEARCH

Frank Laboratory of Neutron Physics

FINAL REPORT ON THE

SUMMER STUDENT PROGRAM

The influence of Sr^{2+} doping on the crystal and magnetic structure of complex iron oxide $Ba_{1-x}Sr_xFe_{12}O_{19}$*: neutron researches*

Supervisor:

Nadezhda Belozerova

Student:

Elvira Mukhametova, Russia
Kazan Federal University

Participation period:

July 01 – August 11

Dubna, 2018

Abstract

Hexagonal ferrites have been widely used as permanent magnets since their discovery. In spite of their relatively modest magnetic properties, hexagonal ferrites of the M-type are still popular in the permanent magnet market because of their low price.

For this reason, an improvement of their magnetic properties by means of incorporation of nonmagnetic cation such as Sr^{2+}, which incite an increase saturation magnetization and at the same time minimizes switching field distribution (SFD) of the particles which is one of a key requirement for high-density recording application is of great relevance.

The crystal and magnetic structure of hexaferrite $Ba_{1-x}Sr_xFe_{12}O_{19}$ (x=0, 0.25, 0.5, 0.75) has been studied by means of a neutron diffraction method on the DN-6 diffractometer at the IBR-2 high-flux pulsed reactor (FLNP JINR, Dubna, Russia) at ambient conditions. Experimental data were analyzed by the Rietveld method using the Fullprof software.

The conservation of the ferrimagnetic structure with substitution has been established. With increasing concentration of Sr^{2+}, the magnetic moments of iron ions in the different crystallographic sites changed no significant.

Parameters of the crystal structure exhibited anisotropic behavior during the changing the concentration of Sr^{2+}. The lattice parameters, interatomic bond lengths and angles, magnetic moments of iron as functions of Sr^{2+} concentration were calculated.

Introduction

In recent years, there has been increasing interest in multiferroic materials. They provide a wide range of potential applications, such as multiple-state memory elements, novel memory media, transducers and new functional sensors. However, materials in which ferroelectricity and ferromagnetism coexist are rare and mostly provide rather weak ferromagnetism.

Since large ferroelectric polarization was found in $PbFe_{12}O_{19}$ ceramics with hexagonal structure, it opened a new direction for potential multiferroic candidate to the conventional ferromagnetic oxides, such as $BaFe_{12}O_{19}$, which holds similar perovskite-like lattice units in its hexagonal structure [1].

M-type barium hexaferrites ($BaFe_{12}O_{19}$) have attracted a lot of attention because of their excellent properties. Barium hexaferrite has high coercive force, large magnetocrystalline anisotropy, high Curie temperature, relatively large magnetization, as well as excellent chemical stability and corrosion resistance [2-6]. As the result, $BaFe_{12}O_{19}$ exhibit potential in great number of applications in various fields. Such hexaferrite is one of the mostly used ferrites in applications as permanent magnets, in magnetic recording media, in microwave devices, and also for fabricating multiferroic devices [1-3].

A significant improvement of the intrinsic magnetic properties of hexaferrites can be obtained by the partial substitution of Sr^{2+} ions [6,7]. Thus, the concentration of Sr^{2+} ions in $Ba_{1-x}Sr_xFe_{12}O_{19}$ compounds determines the magnetic properties of the material such as magnetization, Curie temperature and the magnetocrystalline anisotropy. This is a convenient tool for obtaining a material with the required properties.

Therefore the present work studies crystal and magnetic structure of hexaferrite $Ba_{1-x}Sr_xFe_{12}O_{19}$ (x=0, 0.25, 0.5, 0.75) at ambient conditions.

Physical properties of $BaFe_{12}O_{19}$

$BaFe_{12}O_{19}$ crystallizes in the centrosymmetric magnetoplumbite structure with space group $P6_3/mmc$. As shown in Fig. 1, the magnetic Fe^{3+} ions occupy five different crystallographic sites: tetrahedral ($4f_1$) sites, octahedral sites (2a, $4f_2$, and 12k), and trigonal bipyramidal (TBP) 2b sites[2].

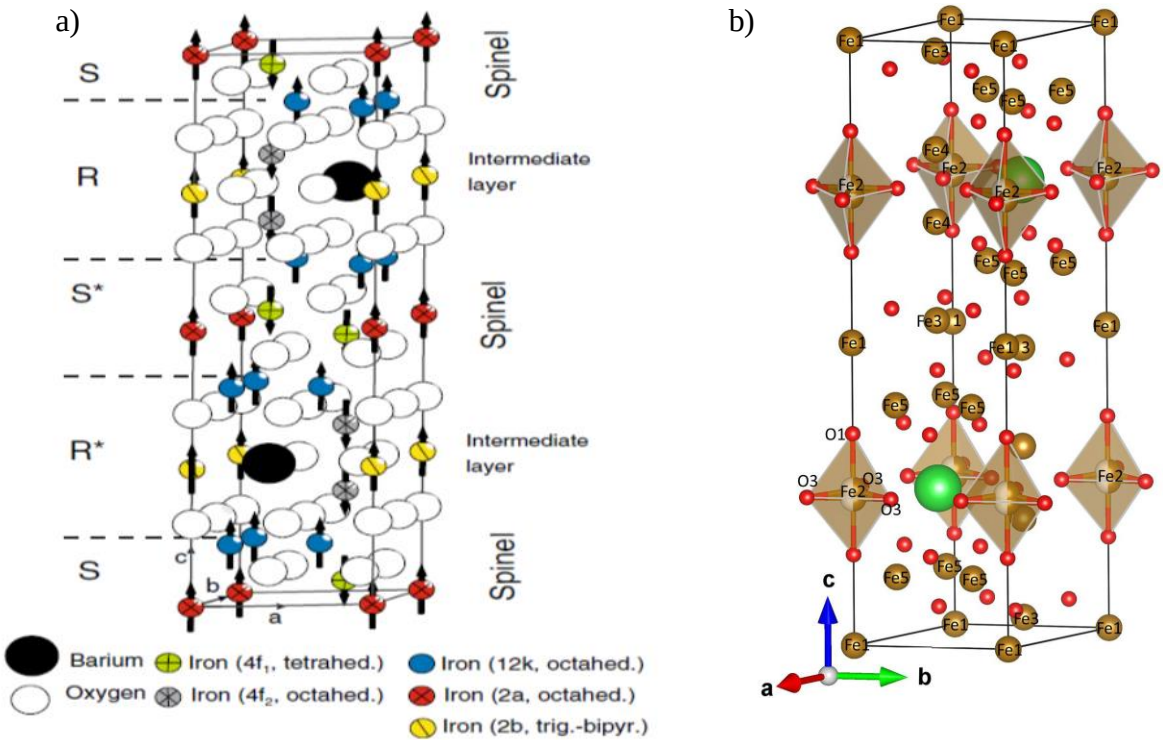

Fig. 1. Crystal Structure of barium hexaferrite (2*$BaFe_{12}O_{19}$) showing a) a unit cell and position of ionic sites in the four spinel blocks (SRS*R*) and relative orientation of magnetic moments of Fe^{3+} ions, b) the nuclear structure of $BaFe_{12}O_{19}$ showing the five Fe sites. The brown balls represent Fe and are labeled by number. The red and green balls represent O and Ba, respectively.

The general structure of M-type hexaferrite ($AO{\cdot}6Fe_2O_3$ or $AFe_{12}O_{19}$, where A is a divalent ion such as Ba^{2+}, Sr^{2+}, Pb^{2+}, etc.) is constructed from 4 building blocks, namely S, S*, R, and R*. The oxygen atoms are closed packed with the A and Fe ions in the interstitial sites. There are ten layers of oxygen atoms along the c axis and the iron atoms are positioned at five crystallographically different sites. The S (Fe_6O_8) and S* blocks are spinels with 2 oxygen layers and six Fe^{3+} ions. Four of these Fe^{3+} ions are in the octahedral sites with their spins aligned parallel to each other. The remaining two Fe^{3+} ions are in tetrahedral sites and have their spins antiparallel to those that are at the octahedral sites. As for the hexagonal R (AFe_6O_{11}) and R* blocks, they consist of three oxygen layers with one of the oxygen anions replaced with an A ion (A= Ba/Sr/Pb). Each R block contains six Fe^{3+} ions, of which five are in octahedral sites, three having spin up and two having spin down polarization. In addition, one of the Fe^{3+} ions is coordinated with five O^{2-} anions and has spin up polarization. The Fe atoms at the 2a site are octahedrally coordinated with equal Fe–O distances, while the octahedrally coordinated Fe ions at $4f_2$ and 12 k sites have different Fe–O interatomic distances. Of the twelve Fe^{3+} ions of the formula unit, the Fe atoms at $4f_1$ sites are tetrahedrally coordinated by oxygen, while the Fe atoms at 2b sites are coordinated by five oxygen ions. There are also short Fe–Fe distances in the structure, and at $4f_2$ sites this Fe–Fe distance is about 2.7 Å.

The Fe ions at 12 k sites form a network with every Fe connected to four other Fe ions in the same layer. In terms of spin, in R block one ion in the 2b layer is up state and two octahedral ions are down state, and in S block seven octahedral ions up state and two tetrahedral ions down state[3].

Structural researches of compounds provide opportunity to study the interrelationship between changes in the structural parameters of the crystal and interatomic distances with changes in the magnetic structure, which is essential in understanding the basic of physical phenomena.

An effective experimental way for obtaining information on the crystal and magnetic structure is the neutron diffraction. Neutron diffraction is unique method. First of all neutrons are sensitive to the light elements such as oxygen, what give opportunity to study crystal structure with high precision. Secondly, the intrinsic magnetic moment make neutrons sensitive to the magnetic structure and dynamics of magnetic substances. Thirdly, the energy of the neutron is comparable with the energy of elementary excitations in the material. This means that, we can obtain information about the dynamics of processes in material[8].

Neutron diffraction

The neutron was discovered by James Chadwick in 1932, and after four years the diffraction of the neutron beam was demonstrated as a result of its scattering by the sample. The concept of Bragg diffraction applies equally to neutron diffraction and electron diffraction processes.

W.H.Bragg, W.L.Bragg and independently of them Y.V. Wulff pointed that a consequence of three dimensional periodicity of a crystal is that it can be divided into various sets of equidistant parallel planes containing identical atomic arrangements. They discovered that the geometry of the X-ray diffraction is similar to the reflection of light by a plane mirror. It is of course follows that the angle between incident ray and reflected ray is 2θ. Thus, the words diffraction and reflection are interchangeable in Wulff - Bragg's law.

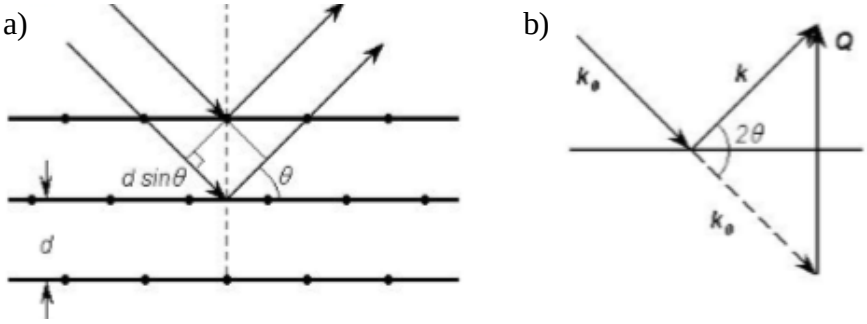

Fig. 2. Bragg reflection from the set of planes with an inter planer spacing of 'd', θ is Bragg angle (a), triangle of neutron scattering (b)[9]

According to Wulff - Bragg's law if the set atomic planes have an inter planer spacing of 'd' and a monochromatic neutron beam of wavelength λ is allowed to incident on the plane with an angle θ and is reflected back with the same angle then for constructive interference between the incident and reflected rays the path difference must be the integral multiple of wavelength i.e.

$$2d \cdot \sin\theta = n\lambda \tag{1.1}$$

where n =0, 1, 2, 3 ... represents the order of reflection, λ is de Broglie wavelength of neutron $\lambda = \frac{h}{mv} = \frac{h}{p} = \frac{h}{\sqrt{2mE}}$

The equation (1.1) is known as Wulff - Bragg's law. That equation can be written in another form, if the total neutron scattering is measured consisting of elastic scattering. It mean, wave vectors of incident and reflected neutrons are equal, and therefore $|\vec{k}| = |\overrightarrow{k_0}|$ (Fig. 1 (b)). Defining the scattering wave vector $\vec{Q} = \vec{k} - \overrightarrow{k_0}$ the diffraction condition can be written as

$$\vec{\mathrm{Q}} = |\vec{k} - \overrightarrow{k_0}| = 2\mathrm{k}\sin\theta = 4\pi \cdot \sin\theta/\lambda, \tag{1.2}$$

where λ is wavelength of incident neutrons. Seeing that the interplanar distance of reciprocal lattice $d = 1/|\vec{H}|$ then

$$\delta(\vec{\mathrm{Q}} - 2\pi{\cdot}n\,\vec{H}). \tag{1.3}$$

Equation (1.3) is another statement for the Wulff-Bragg's law.

Considering the interaction of a neutrons with a nucleus is described by the Fermi potential

$$V = \frac{2\pi h^2}{m} b \cdot \delta(\vec{r} - \vec{R}), \tag{1.4}$$

where $\vec{R}$ is the spatial value of the nucleus. It can be shown that the neutron diffraction cross section on the crystal has the following form

$$\left(\frac{d\sigma}{d\Omega}\right)_{\text{ког}} = \frac{(2\pi)^3}{V_0}\sum_H \delta(\vec{\mathrm{Q}} - 2\pi{\cdot}n) \cdot |\mathrm{F}(\vec{H})|^2, \tag{1.4}$$

where V_0 is volume of unit cell. Thus, the diffraction peaks of neutron scattering, which the intensity goes proportional to $|F(\vec{H})|^2$, will be observed, when the scattering wave vector is a vector of the reciprocal lattice.

$$F(H) = \sum_j b_j \exp(2\pi \cdot i\vec{H}\vec{r_j}), \tag{1.5}$$

where b_j is the coherent amplitudes of neutron scattering, $\vec{r}_j$ is coordinates of atoms in the cell.

Time of flight method

The time of flight (TOF) method is one of the main methods of neutron diffraction analysis. In our days, this is one of the most efficient method in structural neutronography.

The principal schema of a TOF diffraction experiment is shown in Figure 3.

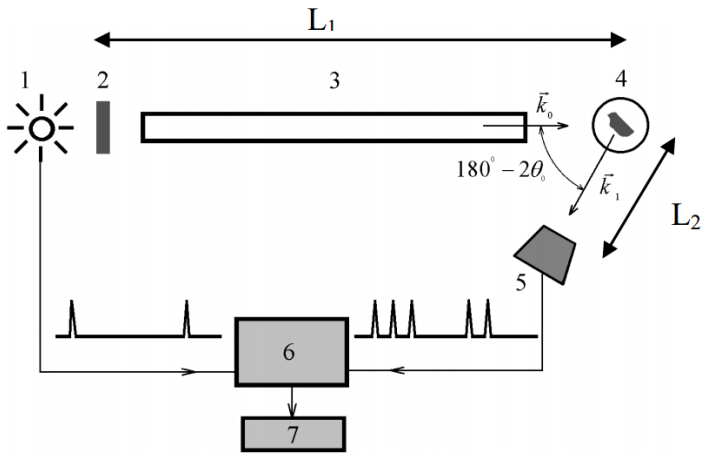

Fig. 3. The lay-out of a TOF diffraction experiment: 1 – pulsed neutron source, 2 – moderator, 3 – flight path of the primary beam, 4 – sample, 5 – detector, 6 – time analyzer, 7 – RW memory[10]

The detector signal is stored in a multichannel time analyzer which is started synchronously with each pulse emission. Thus, the spectrum of recorded counts is built up in dependence on neutron flight time[11].

Neutrons possess the kinetic moment p

$$p = mv = \frac{h}{\lambda}, \tag{1.6}$$

where m is the neutron mass and v its velocity. In this way, the wavelength of neutron

$$\lambda = \frac{h}{mv}. \tag{1.7}$$

On the other hand, the velocity of the neutrons can be obtained from measurement of their flight times (t)

$$v = \frac{L_0 - L_1}{t}. \tag{1.8}$$

The wavelength of neutron can be written as

$$\lambda = \frac{ht}{m(L_0 + L_1)}. \tag{1.7}$$

Reflection occurs from system of parallel crystalline planes with Miller indices (hkl) at a fixed θ_0 and λ. The interplanar distance d_{hkl} should measure up of Wulff-Bragg's low:

$$2d_{hkl} sin\theta_0 = \lambda$$

Combining above equations yields a relation between the time of flight and interplanar d-spacing between lattice planes:

$$d_{hkl} = \frac{ht}{2m(L_0+L_1)sin\theta_0}. \quad (1.8)$$

Scattered neutrons corresponding to the defined d_{hkl} can be easily separate due to the registration time. The time are fixing by the special equipment (time analyzer) which characterized by the number of time channels and they width. The reference-start point is correspond with the special start pulse coincided with neutron flare. Neutron diffraction patterns, obtained such way, represent time-resolved diffraction spectra. The range of wavelengths are widely used on the TOF diffractometeres, generally 0,9 – 8Å, in real life it can achieve 20 Å, which can partially compensate the reduction of neutron flux at long wavelengths.

The resolution of the TOF diffractometer is given as

$$R = \frac{\Delta d}{d} = (\left(\frac{\Delta t}{t}\right)^2 + (ctg\theta\Delta\theta)^2)^{1/2}, \quad (1.9)$$

where Δt is equivocation of time of flight and $\Delta\theta$ is geometric equivocation of dispersal process.

The advantages of TOF-diffraction are manifold increase of the factor of using neutrons from the source in comparison with the other neutron methods and the ability to conduct measurements in a fixed geometry, while working with high pressure cells. The main disadvantage usually is the relatively less precision of the measurements.

Experimental results and discussions

In the present work we analyzed the influence of Sr^{2+} doping on the crystal and magnetic structure of complex iron oxide $Ba_{1-x}Sr_xFe_{12}O_{19}$ (x=0, 0.25, 0.5, 0.75). Neutron powder diffraction measurements for $Ba_{1-x}Sr_xFe_{12}O_{19}$ at room temperature were performed on the DN-6 diffractometer at the IBR-2 high-flux pulsed reactor (FLNP JINR, Dubna, Russia). Diffraction patterns were collected at scattering angle 90° with the resolution Δd/d=0.012 at d=2 Å. Experimental data were analyzed by the Rietveld method using the Fullprof software[12].

Crystal structure

Barium hexaferrite ($BaFe_{12}O_{19}$) has hexagonal structure of *P6₃/mmc (№194)*. The neutron diffraction patterns of $Ba_{1-x}Sr_xFe_{12}O_{19}$ samples evidenced the conservation of initial crystal structure in all Sr^{2+} concentration range (Fig. 4).

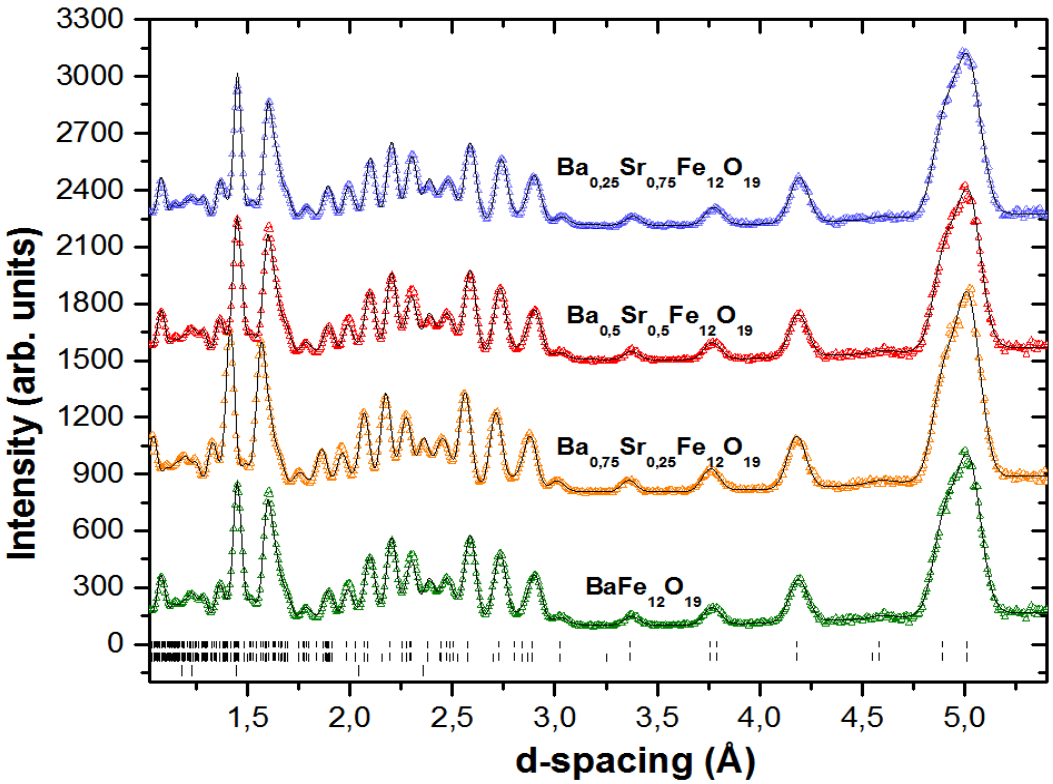

Fig. 4. The neutron diffraction srectra of $Ba_{1-x}Sr_xFe_{12}O_{19}$ (x = 0, 0.25, 0.5, 0.75) obtained at ambient conditions.

The lattice parameters of $Ba_{1-x}Sr_xFe_{12}O_{19}$ (x=0) are a=5.789 Å and c=22.777 Å. These values are in good agreement with accepted literature values [2,4,6]. The refined atomic positions is listed in Table 1.

Table 1: The atomic positions of $BaFe_{12}O_{19}$

Atom	*x*	*y*	*z*
Ba	0.6667	0.3333	0.2500
Fe1	0	0	0
Fe2	0	0	0.2500
Fe3	0.3333	0.6667	0.0280
Fe4	0.3333	0.6667	0.1858
Fe5	0.1689	0.3378	0.8907
O1	0	0	0.1529
O2	0.3333	0.6667	0.9438
O3	0.1959	0.3917	0.2500
O4	0.1547	0.3095	0.0536
O5	0.5018	0.0060	0.1485

Behavior of lattice parameters at different Sr^{2+} concentrations is shown on Fig. 5. The *a* lattice constants increased only slightly, while the *c* parameters diminished significantly. It is the reason of significant changes in exchange interaction of interatomic distances.

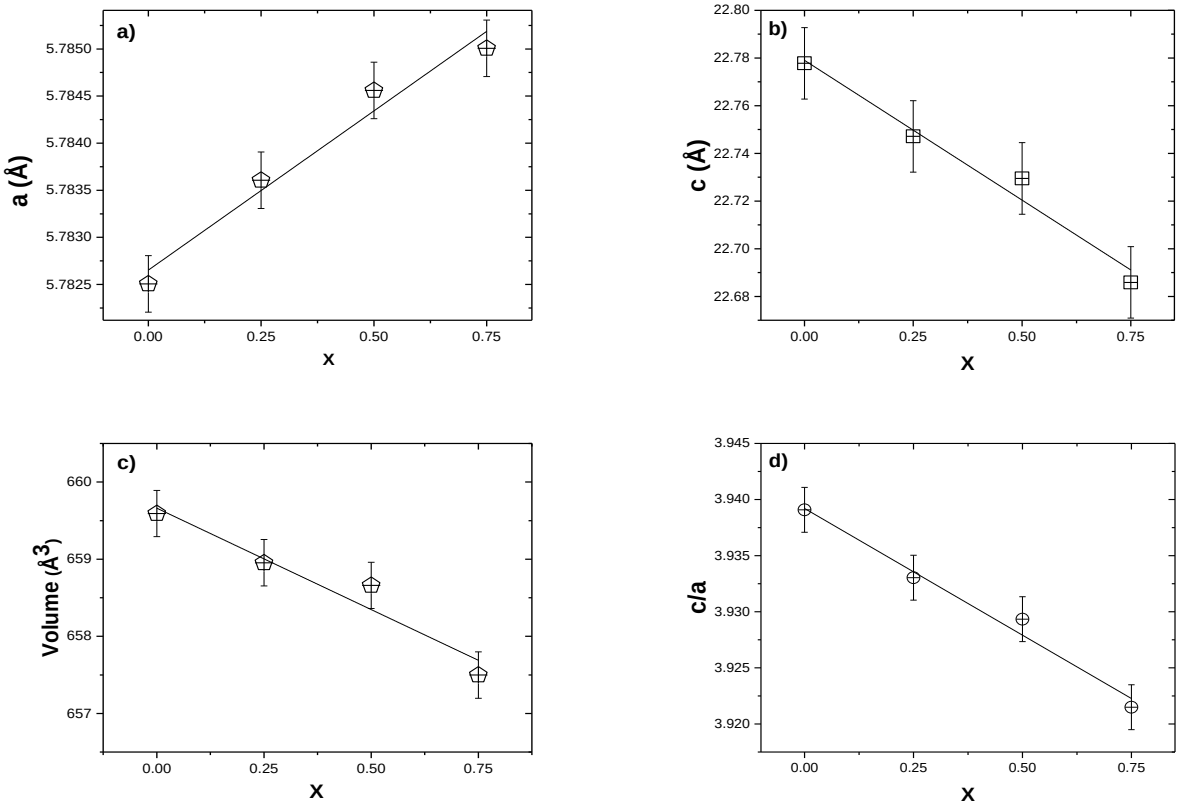

Fig. 5. Composition dependences of cell parameters (a-b), cell volume (c) and ratio c/a in $Ba_{1-x}Sr_xFe_{12}O_{19}$ (x=0, 0.25, 0.5, 0.75)

Interesting features can be revealed by analyzing the variation of the nearest lengths of the Fe–O bond and the Fe-O-Fe bond angles. The values of the bond lengths and angles for $BaFe_{12}O_{19}$ at room temperature presented in Table 2 and Table 3, respectively.

Table 2: The bond lengths for each Fe–O polyhedra of $BaFe_{12}O_{19}$ at room temperature

Bipyramid bond	Length, Å	**Tetra bond**	Length, Å	**Octa bond**	Length, Å	**Octa bond**	Length, Å
Fe2-O1	2.209	Fe3-O2	1.917	Fe1-O4	1.972	Fe5-O1	1.963
Fe2-O3	1.962	Fe3-O4	1.881	Fe4-O3	2.009	Fe5-O2	2.044
				Fe4-O5	1.899	Fe5-O4	2.063
						Fe5-O5	1.864
						Fe5-O5	1.875

Table 3: The Fe-O-Fe bond angles at room temperature of $BaFe_{12}O_{19}$

Bond angle	degrees	**Bond angle**	degrees	**Bond angle**	degrees	**Bond angle**	degrees
Fe1-O4-Fe3	123.761	Fe2-O1-Fe5	120.461	Fe2-O3-Fe4	133.265	Fe3-O2-Fe5	126.336
Fe1-O4-Fe5	96.471	Fe2-O1-Fe5	120.461	Fe2-O3-Fe4	133.264	Fe3-O4-Fe5	121.005
Fe1-O4-Fe5	96.471	Fe2-O1-Fe5	120.461	Fe2-O3-Fe4	133.264	Fe3-O4-Fe5	121.004
Fe2-O1-Fe5	120.461	Fe2-O1-Fe5	120.461	Fe3-O2-Fe5	126.336	Fe4-O5-Fe5	127.457
Fe2-O1-Fe5	120.461	Fe2-O3-Fe4	133.265	Fe3-O2-Fe5	126.337	Fe4-O5-Fe5	126.802

Introduction of Sr^{2+} ions to the $BaFe_{12}O_{19}$ with a smaller atomic radius lead to changes of interatomic distances Fe-O and angles Fe-O-Fe. The influence of Sr^{2+} ions concentration on the behavior of Fe–O bond lengths and bond angles Fe-O-Fe for $Ba_{1-x}Sr_xFe_{12}O_{19}$ (x=0, 0.25, 0.5, 0.75) are shown in the Fig. 6 (a) and (b).

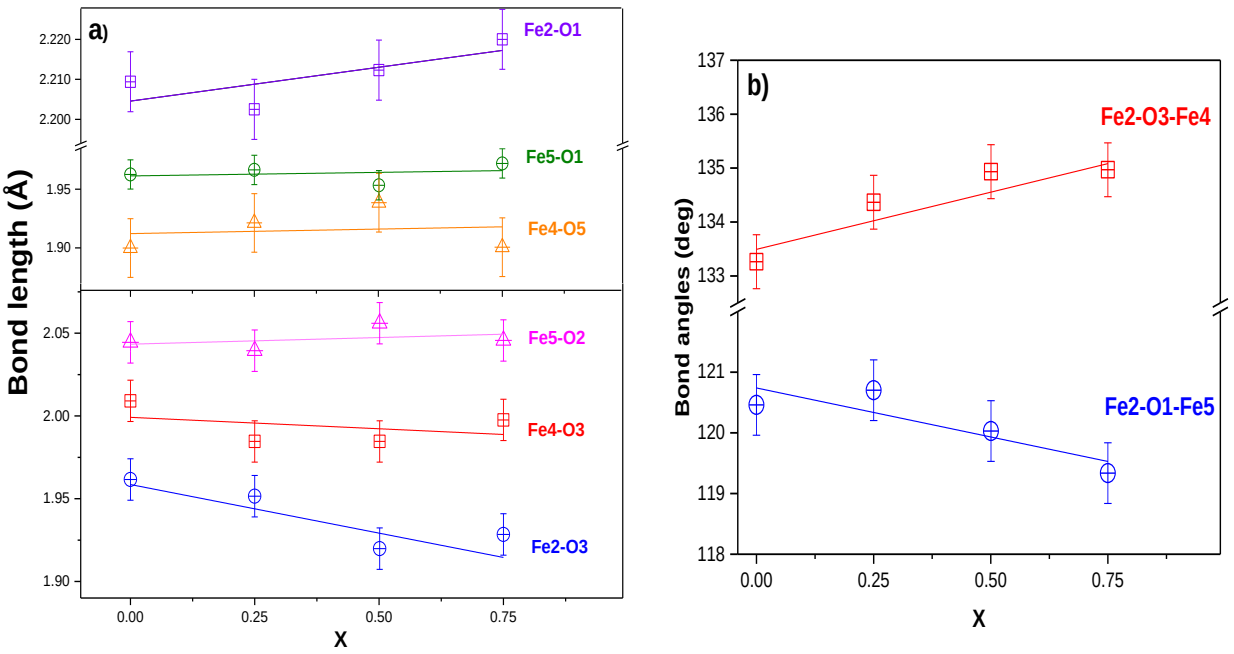

Fig. 6. Composition dependences of the lengths of the nearest Fe–O bonds (a) and the Fe-O-Fe bond angles (b) for the $Ba_{1-x}Sr_xFe_{12}O_{19}$ (x = 0, 0.25, 0.5, 0.75)

The lengths of the bond between iron cations and oxygen anions for most nonequivalent crystallographic sites increase with the doping of Sr^{2+}. However, lengths of the bond decrease for the trigonal bipyramidal (2b), and octahedral ($4f_2$) sites. The change in the lengths of bonds for this sites is opposite. In particular, the lengths of the Fe4–O5 bond for the octahedral site $4f_2$ and the Fe2-O1 bond for the trigonal bipyramidal site 2b increase with substitution Sr^{2+}, whereas the length of the Fe4–O3 bond and Fe2-O3 decrease. The composition dependences of the bond angles Fe2-O3-Fe4 increase with doping Sr^{2+}, at the same time Fe2-O1-Fe5 decrease.

The results of these calculations may indicates a distortion of FeO_5 trigonal bipyramids (TBP). The level of distortion for TBP may be calculate as Δd difference between bond lengths Fe_2-O_1 and Fe_2-O_3. At the room temperature Δd = 0.248 Å for $BaFe_{12}O_{19}$. The value Δd obtained in the present work a little bit bigger than presented in the literature[4]. In addition to it the level of distortion for TBP may be calculate as d_{Fe2-O1}/d_{Fe2-O3}. For the samples $Ba_{1-x}Sr_xFe_{12}O_{19}$ (x = 0, 0.25, 0.5, 0.75) studied in the present work d_{Fe2-O1}/d_{Fe2-O3}=1.126 at room temperature. Distortion of TBP leads to reasonable changes in magnetic structure.

Magnetic structure

The magnetic structure of $Ba_{1-x}Sr_xFe_{12}O_{19}$ (x=0, 0.25, 0.5, 0.75) presented by ferrimagnetic type ordering were found.

The model of the magnetic structure of M-type barium implies that magnetically active Fe^{3+} cations for one formula unit are located at five nonequivalent crystallographic sites, which have tetrahedral (Fe3-4f_1), octahedral (Fe1-2a, Fe4-4f_2, and Fe5-12k), trigonal bipyramidal (Fe2-2b), and oxygen environments (Fig. 1). At the room temperature, 12 Fe^{3+} cations forming five magnetic sublattices are ordered antiparallel (1Fe1↑, 2Fe2↑, 1Fe3↓, 2Fe4↓, 6Fe5↑) and at 0K give the total magnetic moment approximately equal to 20μB per formula unit [13].

The magnetic moment was determined for all nonequivalent crystallographic sites, their values for $BaFe_{12}O_{19}$ at room temperature are listed in Table 4.

Table 4: The magnetic moments of $BaFe_{12}O_{19}$

Atom	Fe1	Fe2	Fe3	Fe4	Fe5
$M_z\ (\mu_B)$	3.690	4.770	3.883	3.291	3.967

Figure 7 shows composition dependences of magnetic moments of iron cations in $Ba_{1-x}Sr_xFe_{12}O_{19}$ (x=0, 0.25, 0.5, 0.75) samples at room temperature.

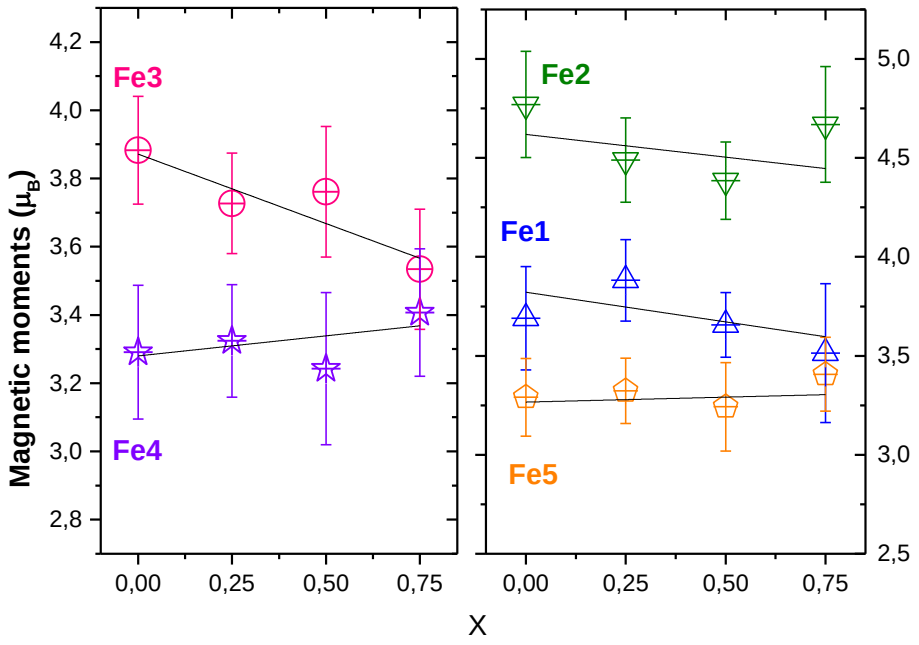

Fig. 7. Composition dependences of magnetic moments of hexaferrite $Ba_{1-x}Sr_xFe_{12}O_{19}$ (x=0, 0.25, 0.5, 0.75) at room temperature.

Introduction of Sr^{2+} ions with a smaller atomic radius strongly influence to the magnetic structure of the $BaFe_{12}O_{19}$. With increasing concentration of Sr^{2+} magnetic moments exhibit anisotropic behavior. The magnetic moments of Fe4 and Fe5 increase gradually with an increase in the substitution concentration of strontium cations, whereas the magnetic moments of Fe1, Fe2 and Fe3 decrease.

The total magnetic moment calculated at room temperature for $Ba_{1-x}Sr_xFe_{12}O_{19}$ (x=0, 0.25, 0.5, 0.75) is 19 μB. This value is in a good agreement with accepted literature values [13].

The influence of Sr^{2+} concentration to the Curie temperature was not studied in the present work.

Conclusion

In this work, we studied the influence of Sr^{2+} doping on the crystal and magnetic structure of complex iron oxide $Ba_{1-x}Sr_xFe_{12}O_{19}$ (x=0, 0.25, 0.5, 0.75). Neutron powder diffraction measurements for $Ba_{1-x}Sr_xFe_{12}O_{19}$ were performed on the DN-6 diffractometer at the IBR-2 high-flux pulsed reactor (FLNP JINR, Dubna, Russia). Experimental data were analyzed by the Rietveld method. In the course of the work, the technique of processing experimental data and FullProof software were mastered. The main characteristics of crystal and magnetic structure were calculated for different compositions of samples. The lattice parameters, cell volume, bond distances between oxygen and iron in three different positions were determined for each diffraction spectrum. The lattice parameters and bond distances have an anisotropic behavior with increasing of Sr^{2+} concentration.

The conservation of the ferrimagnetic structure with substitution has been established. The magnetic moment was determined for all nonequivalent crystallographic sites for $Ba_{1-x}Sr_xFe_{12}O_{19}$ (x=0, 0.25, 0.5, 0.75).

Acknowledgement

I take this opportunity to express my profound gratitude and deep regards to my supervisor N. M. Belozerova for her exemplary guidance, monitoring and constant encouragement throughout the course of this project.

I also take the opportunity to express a deep sense of gratitude to A.V. Rutkauskas and the team of high pressure research for their valuable information and guidance which helped me completing this task through various stages.

Lastly, I would like to thank a committee of Summer Student Program for opportunity to visit Joint institute for nuclear research and for financial support.

References

1. G. Tan, X. Chen, Journal of Magnetism and Materials 327, 87-90 (2013).
2. H.B. Cao, Z.Y. Zhao, M. Lee et al., APL Materials 3, 062512 (2015).
3. S.E. Jacobo, P.G. Bercoff, Solid State Phenomena 202, 113-125 (2013).
4. W.D. Townes, J.H. Fang, A.J. Perrota, Zeitschrift für Kristallographie 125, 437-449 (1967).
5. V.A. Bokov, St. Petersburg.: The Neva dialect, 272 (2002).
6. F. M. M. Pariera, C. A. R. Junior, M. R. P. Santos et al., J Mater Sci: Mater Electron 19, 627-638 (2008).
7. X. Obradors, X. Solans, D. Samaras et al. JOURNAL OF SOLID STATE CHEMISTRY 72, 218-224 (1988).
8. V.A. Cherepanov, URGU, 104 (2007).
9. A.V. Belushkin, MSU, 167 (2000).
10. V.L. Aksenov, A.M. Balagurov, Physics-Uspekhi 166, 955-985 (1996).
11. K. Feldmann, Texture and Microstructures 10, 309-323 (1989).
12. J.Rodriguez-Carvajal, Physica B 192, 55 (1993).
13. S.V. Trukhanov, A.V. Trukhanov, V.G. Kostishin, JETP Letters 103, 2 (2016).